Long-range antiferromagnetic ordering in the $S=\frac{1}{2}$ ordered rocksalt oxide Li_5OsO_6: Comparison with the isoelectronic and isostructural spin glass Li_4MgReO_6

Shahab Derakhshan* and John E. Greedan
Brockhouse Institute for Materials Research and Chemistry Department, McMaster University, 1280 Main Street West, Hamilton, Ontario L8S 4M1, Canada

Lachlan M. D. Cranswick
Canadian Neutron Beam Centre, National Research Council Canada Building 459, Chalk River Laboratories, Chalk River, Ontario K0J 1J0, Canada

(Received 1 October 2007; revised manuscript received 15 November 2007; published 4 January 2008)

Li_5OsO_6 and Li_5ReO_6 polycrystalline samples were synthesized by conventional solid state methods. Employing powder neutron diffraction data, the crystal structure of Li_5OsO_6 was reinvestigated. Li_5OsO_6 crystallizes in $C2/m$ in an ordered NaCl structure type, where $a=5.0472(1)$ Å, $b=8.7827(2)$ Å, $c=5.0079(1)$ Å, $\beta=109.777(2)°$ and $V=208.90(1)$ Å^3. Magnetic susceptibility and heat capacity data indicate an antiferromagnetic long-range order below 40 K, although there is evidence for low dimensional short-range order below 80 K. As well, the frustration index, $f=|\theta|/T_N\sim 1$, in contrast to the isostructural and isoelectronic compound, Li_4MgReO_6, which is a spin glass below 12 K and has $f\sim 14$. An attempt was made to rationalize these differences using spin dimer analysis. The key results are that the spin exchange interactions in the Re-based compound are stronger and are consistent with a frustrated triangular lattice model, while a low dimensional short-range order model is better for Li_5OsO_6. The main reason for this is a strong *Jahn-Teller* distortion in the OsO_6 octahedron material which constrains the unpaired electron to occupy the d_{xy} orbital.

DOI: 10.1103/PhysRevB.77.014408 PACS number(s): 75.50.Ee

I. INTRODUCTION

Antiferromagnetic (AFM) compounds with a triangular cationic sublattice have the potential to exhibit magnetic frustration, as the three exchange interactions cannot be satisfied simultaneously.[1] Such systems with $S=\frac{1}{2}$ have been considered as spin-liquid ground state candidates.[2]

Ordered rocksalt type transition metal oxides[3] comprise such lattices and are interesting from this point of view. $LiNiO_2$ (Refs. 4 and 5) and $NaTiO_2$ (Ref. 6) have been considered as candidates for a spin-liquid magnetic ground state. While $Na_3Co_2SbO_6$ (Ref. 7) with a honeycomb lattice exhibits AFM long-range order, isostructural $Na_3Cu_2SbO_6$ (Ref. 8) has a singlet ground state with spin gap behavior and is best defined based on a short-range AF-AF one-dimensional alternate chain model.[9]

In contrast to the 3*d* transition metal oxides, the physical properties of 4*d* and 5*d* compounds have not been widely studied. The latter compounds have more extended *d* orbitals and also exhibit large spin-orbit coupling. Accordingly, they usually behave differently from the 3*d* systems. Na_3RuO_4 (Ref. 10) exhibits three-dimensional magnetic ordering with some degrees of frustration. Furthermore, Li_4MgReO_6 (Ref. 11) shows spin-glass behavior below 12 K and not long-range order. The chemistry of osmium oxides is very rich as Os can take a wide range of valence numbers, namely, +4 to +7. Among the Os^{7+} compounds, Ba_2LiOsO_6 undergoes a long-range AFM ordering below 8 K with some evidence of frustration whereas Ba_2NaOsO_6 shows FM behavior.[12,13]

The physical properties of the title compound, Li_5OsO_6,[14] which is isostructural and isoelectronic with Li_4MgReO_6, have not been investigated in detail. The existing, but sparse,

TABLE I. The values for the ζ_i coefficients and valence shell ionization potentials H_{ii} of the STO's employed for the spin dimer calculations for Li_5OsO_6 and Li_4MgReO_6.

Atom	Orbital	H_{ii} (eV)	ζ_i	C	ζ_i'	C'
O	2*s*	−32.300	2.688	0.7076	1.675	0.3745
O	2*p*	−14.8000	3.694	0.3322	1.659[a]	0.7448
Os	6*s*	−8.170	2.400	1		
Os	6*p*	−4.810	1.770	1		
Os	5*d*	−11.840	4.504	0.6066	2.391	0.5486
Re	6*s*	−9.360	2.346	1		
Re	6*p*	−5.960	1.730	1		
Re	5*d*	−12.660	4.339	0.5886	2.309	0.5627

[a]This value corresponds to the diffuse STO of O 2*p* when $x=0$.

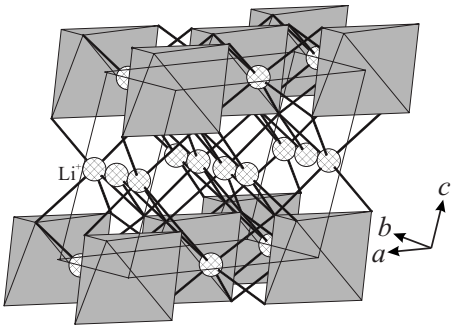

FIG. 1. Edge-sharing octahedra in Li_5OsO_6 viewed. The gray octahedra represent $[OsO_6]^{5-}$ and the circles are Li^+ ions.

magnetic susceptibility data indicate a possible anomaly near 40 K. In this paper, the temperature dependent magnetic susceptibility and heat capacity data for Li_5OsO_6 are measured and are compared to those of Li_4MgReO_6. Moreover, to understand the driving force for the different magnetic properties between two systems, the calculated relative magnitudes of the different spin exchange interactions for both compounds are also presented.

II. EXPERIMENTAL SECTION

A. Synthesis

The starting material, Li_2O, was prepared by heating lithium hydroxide monohydrate (Frederick Smith Chemicals, 98%) to 450 °C in a fused silica tube under dynamic vacuum for 18 h. The Li_5OsO_6 sample was prepared according to the procedure introduced by Betz *et al.*[14] For this purpose, a stoichiometric mixture of Li_2O and Os (Alfa Aesar, 99.95%) powder was thoroughly ground and pressed into a pellet in an argon filled glove box. The pellet was placed in an alumina boat and heated to 500 °C in a tube furnace under dynamic argon flow; after 5 h, the argon flow was switched to oxygen flow and the sample was heated to 800 °C for 12 h and was cooled to room temperature in 10 h.

TABLE II. Some selected structural parameters of Li_5OsO_6 and Li_4MgReO_6.

	Li_5OsO_6	Li_4MgReO_6[a]
a (Å)	5.0472(1)	5.0979
b (Å)	8.7827(2)	8.8163
c (Å)	5.0079(1)	5.0815
β (deg)	109.777(2)	109.835
V (Å^3)	208.90(1)	214.83

[a]Reference 11.

For preparing Li_5ReO_6, a stoichiometric mixture of Li_2O and Re_2O_7 (CERAC, 99.99%) powder was pressed into a pellet, which was placed in a platinum boat and heated to 900 °C in a tube furnace under dynamic oxygen flow. After 18 h, the furnace was turned off.[15]

B. Phase analyses

The formation and phase purity of the black Li_5OsO_6 and yellow Li_5ReO_6 products were confirmed using powder x-ray diffraction, employing a Guinier-Hägg camera with Cu $K\alpha_1$ radiation and Si as the internal standard. To convert the film record to digital data, a KEJ line scanner was utilized.

C. Crystal structure and magnetic structure determination using neutron diffraction

Powder neutron diffraction measurements at different temperatures were performed on the C2 diffractometer at the Canadian Neutron Beam Centre at Chalk River, Ontario. The room temperature data were collected using two different wavelengths of 1.3307 Å in the angular range of $36° \leqslant 2\theta \leqslant 113°$ with 0.1° steps and 2.3724 Å in the angular range of $10° \leqslant 2\theta \leqslant 82°$.

Low temperature data (3 K) were collected for investiga-

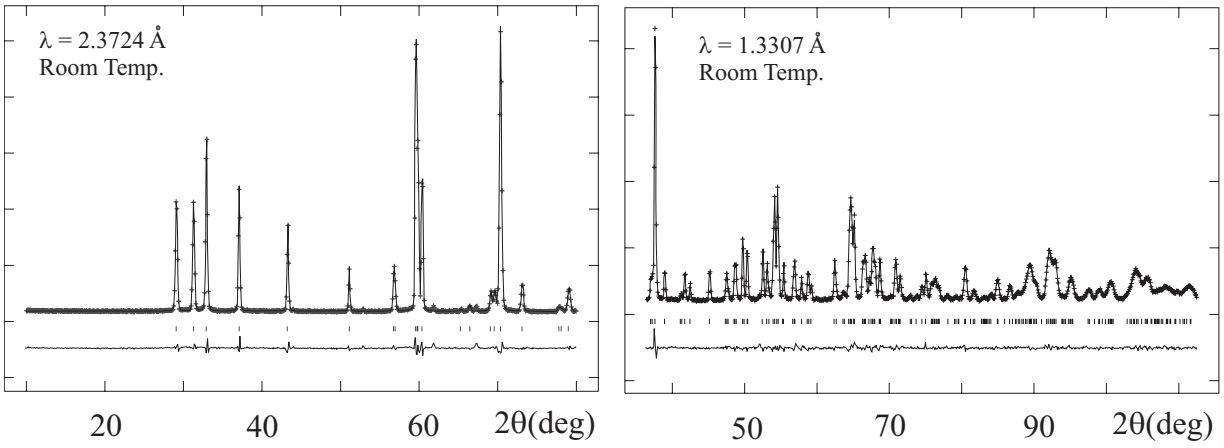

FIG. 2. Room temperature neutron diffraction pattern using long wavelength (left) and short wavelength (right) neutrons. The cross points indicate the experimental data, the solid line represents the Rietveld fit, and the thin lines below the pattern the difference. The expected peak positions are shown by the tick marks.

TABLE III. Atomic coordinates and equivalent isotropic displacement parameters for Li_5OsO_6.

	X	Y	Z	U_{iso} (Å^2)
Os	0	0	0	0.0057(3)
Li1	0	0.6733(8)	0	0.013(1)
Li2	0	0.5	0.5	0.014(2)
Li3	0.5	0.3148(7)	0.5	0.014(2)
O1	0.2688(4)	0.3467(2)	0.7634(3)	0.0068(4)
O2	0.2741(5)	0.5	0.2229(4)	0.0099(6)

tion of the magnetic structure, using the long wavelength 2.36957 Å in the range of $5° \leqslant 2\theta \leqslant 82°$ with 0.1° interval.

D. Physical properties measurements

Temperature dependent magnetic susceptibility data for a Li_5OsO_6 powder sample, encased in a gelatin capsule, were collected employing a Quantum Design MPMS SQUID magnetometer. Both zero-field cooled (ZFC) and field cooled (FC) data were obtained over the temperature range of 5–300 K at an applied field of 1000 Oe. Diamagnetic corrections were added to the susceptibility data.

Heat capacity data were collected from 5 to 60 K using the heat capacity probe of the Oxford MagLab system, without applying any external magnetic field. The powder sample was pressed into a thin pellet and a small portion of that was resintered to minimize the grain boundaries. The thin block was mounted onto a sapphire measurement chip with Apeizon grease. Contributions to the measured heat capacity by the grease and sample holder chip were calibrated.

E. Theoretical calculations; Spin dimer analyses

To estimate the relative values of the various exchange constants J's, extended Hückel, spin dimer analysis[16] was performed. In these computations, two OsO_6^{5-} units ($Os_2O_{12}^{10-}$ dimer) for each pathway were taken into account and the intersite hopping energy (Δe) was estimated using the CAESAR package.[17] Double-zeta Slater type orbitals (STOs) were employed for the oxygen s and p and osmium d states and single-zeta for osmium s and p states. The values of the ζ_i and ζ_i' coefficients and valence shell ionization potentials H_{ii} used for the calculations are presented in Table I.

TABLE IV. Some selected interatomic Os-O and Re-O distances of Li_5OsO_6 and Li_4MgReO_6.

Li_5OsO_6		Li_4MgReO_6[a]	
4×Os-O (Å)	1.9083(1)	4×Re-O (Å)	1.9622
2×Os-O (Å)	1.8459(2)	2×Re-O (Å)	1.9323

[a]Reference 11.

For d^1 systems, the tetragonal compression Jahn-Teller effect is expected, where the d_{xy} state lies below the d_{xz} and d_{yz} states. In extreme conditions the d_{xy} state is well separated from the other states and exclusively accommodates the unpaired electron. In this case, there is only one interaction, which is responsible for the magnetic interaction and assuming that $J \cong (\Delta e)^2/U$ and that U is constant, the relative magnitude of the various J's can be determined.

Alternatively, if the energy separations between these states are small, the probability of the d_{xz} and d_{yz} states to be occupied will be high and they can also contribute to the spin exchange interactions. In the simplest case, the probability that d_{xy}, d_{xz}, and d_{yz} contribute to the exchange interactions is equal and we have

$$\langle (\Delta e)^2 \rangle \approx \frac{1}{N^2} \sum_{\mu=1}^{N} (\Delta e_{\mu\mu})^2. \quad (1)$$

In these systems, there are three states which are involved and therefore Eq. (1) can be rearranged as

$$\langle (\Delta e)^2 \rangle \approx \frac{1}{9}[(\Delta e_{11})^2 + (\Delta e_{22})^2 + (\Delta e_{33})^2], \quad (2)$$

and finally the spin exchange interactions will be given by

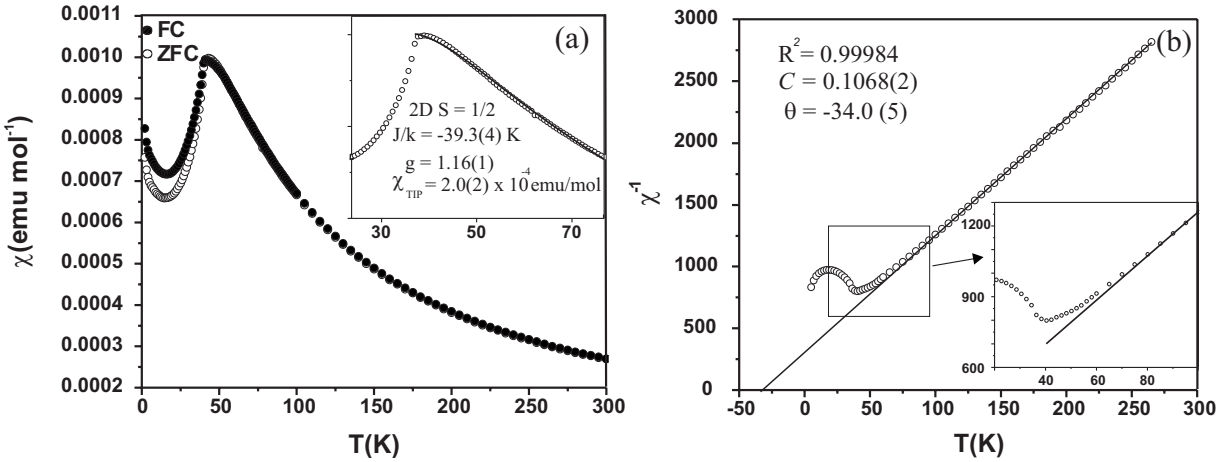

FIG. 3. (a) Zero-field cooled and field cooled magnetic susceptibility data for Li_5OsO_6. The open circles represent the ZFC data and the filled circles represent the FC data. (b) Curie-Weiss fit in the high temperature, paramagnetic, region. The open circles represent the ZFC data points and the solid line is the fit. The insets show evidence for short-range correlations which are described in the text.

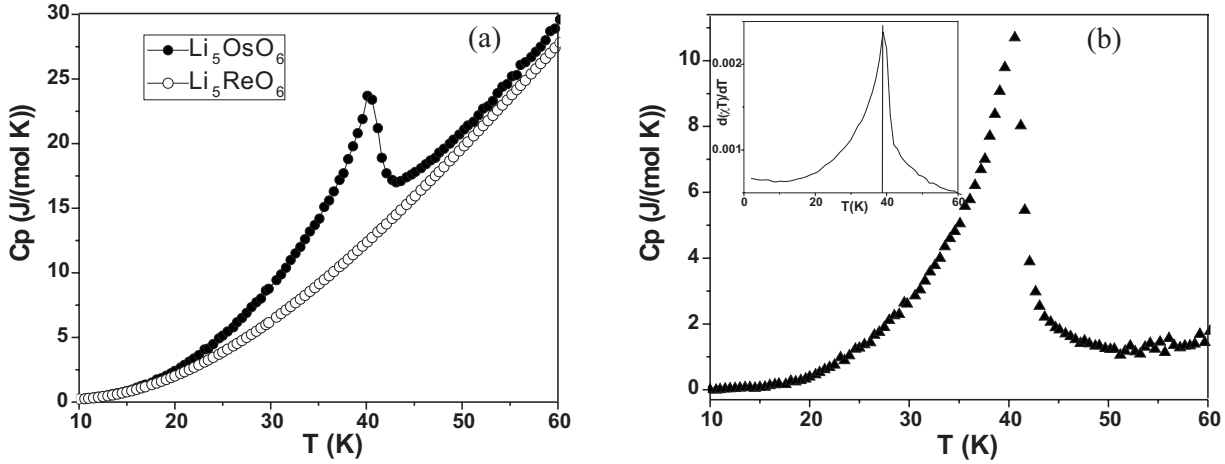

FIG. 4. (a) Temperature dependent heat capacity data for Li_5OsO_6 (filled circles) and the lattice match Li_5ReO_6 (open circles). (b) The difference plot represents the electronic contribution to the heat capacity, which is in a very good agreement with Fisher heat capacity analyses (inset plot) using magnetic data.

$$J \cong \frac{\langle (\Delta e)^2 \rangle}{U}. \tag{3}$$

The corresponding relative exchange interactions for both Re- and Os-based compounds were calculated according to both the above-mentioned approaches. To examine the consistency of the calculations, different values of $(1-x)\zeta_i'$ with $x=0$, 0.05, and 0.1 for oxygen $2p$ atomic orbitals were employed. ζ_i' describes the diffuse STO and by providing an orbital tail enhances the overlap between oxygen atoms within the super-super-exchange (SSE) pathways.[18] To compare the relative strengths of the Jahn-Teller effect for these two systems, extended Hückel molecular orbital calculations for $[OsO_6]^{5-}$ and $[ReO_6]^{6-}$ species were performed as well.

III. RESULTS AND DISCUSSION

A. Crystal structure

Li_5OsO_6 crystallizes in $C2/m$ in an ordered form of the rocksalt structure type (Fig. 1). The structure is composed of edge shared octahedra where one layer has the composition of $Li_2OsO_6^{3-}$ and the other layer only contains Li^+ cations (LiO_6 octahedra).

To investigate the crystal structure, Rietveld refinements were performed on the room temperature neutron diffraction data sets using the GSAS program.[19,20] The cell parameters and atomic positions were initially taken from the proposed model by Betz *et al.*[14] A pseudo-Voigt peak shape profile, which is composed of both Gaussian and Lorentzian parameters, was chosen and the parameters were refined to obtain the best fit to the experimental data. The space group is $C2/m$, with lattice dimensions of $a=5.0472(1)$ Å, $b=8.7827(2)$ Å, $c=5.0079(1)$ Å, $\beta=109.777(2)°$, and $V=208.90(1)$ Å^3, with residual factors of $Rp=0.032$ and $wRp=0.042$ (Fig. 2). Li_5OsO_6 is isostructural to Li_4MgReO_6.[11] In addition to the fact that Li_5OsO_6 has a smaller cell volume than Li_4MgReO_6, the major structural difference is that the three independent crystallographic positions for Li in Li_5OsO_6 exhibit mixing between Li and Mg in Li_4MgReO_6. The crystallographic details and the atomic positions are summarized in Tables II and III. Some selected interatomic distances are presented in Table IV. In both Li_5OsO_6 and Li_4MgReO_6, the $Os(Re)O_6$ octahedra exhibit a tetragonal compression, with two bonds shortened, which may be due to a Jahn-Teller distortion which is expected for a d^1 electronic configuration. This feature is evidently more pronounced in Li_5OsO_6.

B. Magnetic susceptibilities

In the low temperature data (5–100 K), the sharp increase in susceptibility at low temperature (5–20 K) regime (Fig. 3) can be attributed to a paramagnetic impurity. A sharp lambda-shaped peak in the susceptibility with a maximum near 40 K is indicative of the long-range antiferromagnetic nature of the magnetism of this compound.

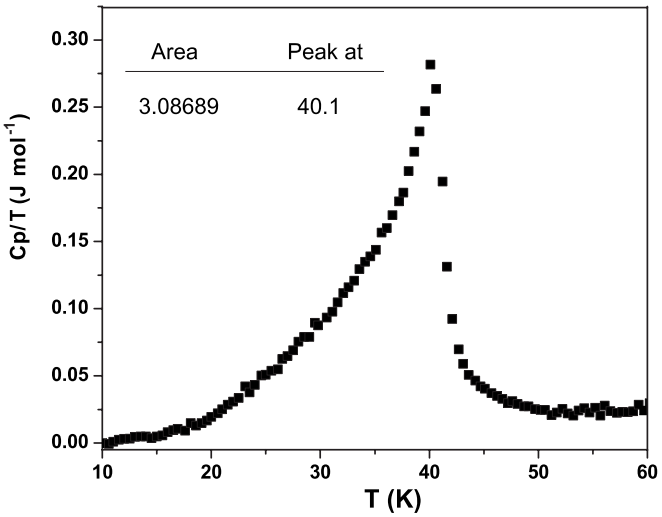

FIG. 5. C_P/T as the function of the temperature. The area under the peak represents the entropy for the magnetic transition in Li_5OsO_6.

TABLE V. Comparison of relevant magnetic parameters for Li_4MgReO_6 and Li_5OsO_6.

	Li_4MgReO_6	Li_5OsO_6
μ_{eff} (μ_B)	1.14	0.92(4)
θ (K)	−166(3)	−34.0(5)
$T_{N,g}$	~12	40
Ground state	Spin glass	AF LRO
F	~14	~1

The high temperature magnetic susceptibility data of Li_5OsO_6 from 100 to 300 K [Fig. 3(b)] were seen to fit very well to the Curie-Weiss law, $\chi = C/T - \theta$. The fitting parameters are $C = 0.1068(2)$ emu/mol for the Curie constant and $\theta = -34.0(5)$ K for the Weiss constant. This Curie constant corresponds to an effective magnetic moment μ_{eff} of $0.92(4)\mu_B$ per Os^{7+} $(5d^1, S=\frac{1}{2})$, which is lower than the spin-only value of $1.73\mu_B$. This is in agreement with the fact that the magnetic moment of the heavy cations, such as Os^{7+}, is strongly influenced by orbital contributions as well, and spin-orbit coupling in the electronic configurations less than half filled is in the form of L-S. This results in a magnetic moment with a lower value than that of the spin-only case. The negative value for the Weiss constant is indicative of predominant AF interactions.

The relationship between the Weiss temperature and the various exchange constants J_m is well known and given as Eq. (1) by the mean field theory:[21]

$$\theta = \frac{2S(S+1)}{3k_B} \sum_{m=1}^{N} z_m J_m, \tag{4}$$

where θ is the Weiss constant, z_m is the number of mth nearest neighbors of a given atom, J_m is the exchange interaction between mth neighbors, and N is the number of sets of neighbors for which $J_m \neq 0$. The Weiss temperature sets the scale for the magnetic exchange energy in a system. In general, large exchange energies result in relatively high Neél temperatures, unless some other factors such as frustration prevents the ordering and lowers the transition temperature. It is common to apply the so-called frustration index, $f \sim \frac{|\theta|}{T_N}$, to determine the level of magnetic frustration in a material.[22] Systems showing $f > 5$ are considered frustrated and therefore Li_5OsO_6 with $f \sim 1$ is not a frustrated system. As will be discussed later, this is in stark contrast to the situation for Li_4MgReO_6.

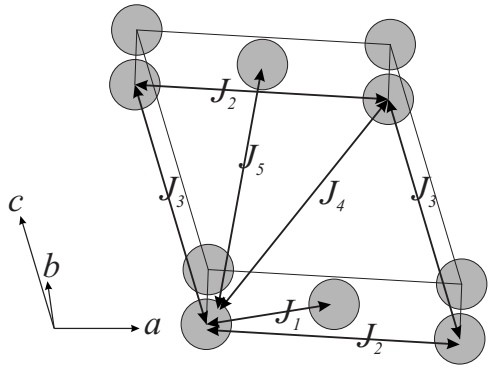

FIG. 6. Schematic representation of different possible Os-Os interaction pathways in the unit cell.

TABLE VI. The relevant distances to the five identified exchange pathways, J_1, J_2, J_3, J_4, and J_5.

	M=Os	M=Re[a]
(M-M)[J_1] (Å)	5.065	5.0920
(M-M)[J_2] (Å)	5.047	5.098
(M-M)[J_3] (Å)	5.008	5.082
(M-M)[J_4] (Å)	5.783	5.851
(M-M)[J_5] (Å)	6.495	6.554

[a]Reference 11.

C. Heat capacity data

The temperature dependent heat capacity data of Li_5OsO_6 are shown in Fig. 4(a) as black circles. A lambda-shaped anomaly is seen near 40 K, which is additional proof for the long-range magnetic order at this temperature. Heat capacity is composed of both electronic and phonon (lattice) contributions. To eliminate the lattice component, we collected comparable data for Li_5ReO_6 [open circles in Fig. 4(a)]. This material was the best choice for this purpose as (1) it crystallizes in the same structure type; (2) the electronic configuration of Re^{7+} is $[Xe]5d^0\ 6s^0$ and there is no unpaired electron in the outer shell to contribute in heat capacity; (3) Re is adjacent to Os in Periodic Table and the mass difference is minimized.

Subtracting these data sets, the electronic contribution to the heat capacity of Li_5OsO_6 was obtained [Fig. 4(b)]. Note the remarkable accordance with the Fisher heat capacity analysis[23] [the inset in Fig. 4(b)] using magnetic susceptibility data. For this purpose, the derivative $d(\chi T)/dT$ is plotted, which gives a good approximation to the magnetic component of the heat capacity.

One can calculate the entropy associated with the transition using Eq. (5):

$$\Delta S_{\text{exp}} = \int_0^T \left(\frac{C_P}{T}\right) dT, \tag{5}$$

TABLE VII. The relevant (M-O-O) angles to the five identified exchange pathways, J_1, J_2, J_3, J_4, and J_5.

	M=Os	M=Re[a]
(<M-O-O)[J_1] (deg)	136.63	136.75
(<M-O-O)[J_2] (deg)	91.49	96.51
(<M-O-O)[J_3] (deg)	92.19	90.95
(<M-O-O)[J_4] (deg)	135.11	135.68
(<M-O-O)[J_5] (deg)	140.01	137.57

[a]Reference 11.

TABLE VIII. $(\Delta e)^2$ for the various exchange pathways in both Li_5OsO_6 and Li_4MgReO_6 calculated on the spin dimer model assuming d_{xy} occupation only.

Pathway	$Li_5OsO_6(\Delta e)^2$ $(meV)^2$	Rel.	$Li_4MgReO_6(\Delta e)^2$ $(meV)^2$	Rel.
J_1	68.91	0.022	238.08	0.049
J_2	0.14	0.00005	0.18	0.00004
J_3	0.04	0.00001	1.32	0.0003
J_4	3102.82	1	4854.74	1
J_5	57.76	0.019	74.29	0.015

Accordingly, the peak area in Fig. 5 is the experimental entropy associated with the magnetic phase transition within the temperature range (10–60 K), which is 3.09 J/mol K. On the other hand, Boltzmann's law gives the overall theoretical transition entropy:

$$\Delta S_{\text{theor}} = R \ln \omega,$$

where ω is spin multiplicity; $2S+1=2$ and therefore,

$$\Delta S_{\text{theor}} = 5.76 \text{ J/mol K},$$

$$\frac{\Delta S_{\text{exp}}}{\Delta S_{\text{theor}}} = \frac{3.09}{5.76} = 0.54.$$

So, only 54% of the total transition entropy is lost below the magnetic phase transition which suggests the importance of some short-range interactions at higher temperatures.

Corroborating evidence for short-range magnetic correlations can be found from Fig. 3. Note [inset of Fig. 3(b)] that deviations from the Curie-Weiss law set in below ~80 K, a factor of 2 greater than T_N. As well [Fig. 3(a)] the susceptibility just above T_N is convex upward, a typical signature of short-range AFM correlations. The data within the interval 40–80 K could be fitted to various $S=\frac{1}{2}$ one-dimensional (1D) or two-dimensional (2D) models [a 2D fit is shown in the inset to Fig. 3(a)] giving roughly equal residuals and $J_{\text{SRO}}/k_B \approx -40$ K (2D) or ≈ -30 K (1D). While this observation is strong support for the importance of antiferromagnetic SRO in Li_5OsO_6, it is not possible to assign a specific model given the relatively narrow temperature range and the absence of a well-defined susceptibility maximum. The computational results to be described in Sec. III E support a low dimensional model for the short-range correlations rather than a geometrically frustrated model.

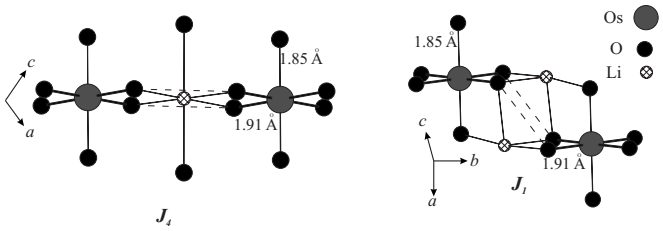

FIG. 7. The detailed J_1 and J_4 SSE pathways. The long and short $M-O$ bonds are shown by the thick and thin lines, respectively. The O-O interactions are denoted by the dashed lines. The four oxygen, two osmium, and the lithium atom, which are involved in the J_4 pathway (left) are coplanar. The J_1 pathway (right) does not fulfill this condition.

D. Comparison of Li_5OsO_6 with Li_4MgReO_6

Given that Li_5OsO_6 is isostructural and isoelectronic with the previously studied Li_4MgReO_6 and both are $S=\frac{1}{2}$ spin systems, a detailed comparison is in order. Table V shows a comparison of parameters relating to the issues of frustration and the nature of the magnetic ground state.

While there is one similarity, the effective magnetic moment is strongly reduced for both materials from the spin-only value of $1.73\mu_B$, due to the effects of spin-orbit coupling, in most cases the two materials are profoundly different. Li_4MgReO_6 is spin-glass-like below 12 K with a very large, negative $\theta=-166$ K and a high frustration index of ~14. The Os-based material is, on the other hand, a more or less conventional antiferromagnet with $T_N \sim 40$ K and a frustration index near unity. This raises questions as to what are the factors which cause such a remarkable contrast in the properties of two isoelectronic and isostructural compounds.

E. Computational methods

1. Tight binding, magnetic dimer model

All the possible spin exchange interaction pathways are presented in Fig. 6. All these pathways are SSE and their

TABLE IX. $\langle(\Delta e)^2\rangle$ for the various exchange pathways in both Li_5OsO_6 and Li_4MgReO_6 calculated on the spin dimer model, assuming that the occupation of the d_{xy}, d_{xz}, and d_{yz} orbitals are equally probable.

	Li_5OsO_6						Li_4MgReO_6					
	$\langle\Delta e\rangle$ $(meV)^2$			Rel.			$\langle\Delta e\rangle$ $(meV)^2$			Rel.		
x[a]	0	0.05	0.10	0	0.05	0.10	0	0.05	0.10	0	0.05	0.10
J_1	20	48	189	0.03	0.03	0.04	51	79	428	0.06	0.03	0.08
J_2	710	1800	4128	1	0.96	0.95	893	2320	5374	1	1	1
J_3	310	1881	4334	0.44	1	1	723	1890	4492	0.81	0.81	0.84
J_4	420	888	1865	0.59	0.47	0.43	626	1343	2648	0.70	0.58	0.49
J_5	18	42	78	0.03	0.04	0.02	27	69	133	0.03	0.03	0.02

[a] x is the modification factor for the diffuse STO exponent of O $2p$ in the form of $(1-x)\times\zeta_i'$.

TABLE X. The molecular orbital energies of 6*d* states for $[OsO_6]^{5-}$ and $[ReO_6]^{6-}$ octahedra.

	25 (eV)	26 (eV)	27 (eV)	28 (eV)	29 (eV)
$[OsO_6]^{5-}$	−10.003	−9.814	−9.809	−2.208	−0.965
$[ReO_6]^{6-}$	−10.545	−10.464	−10.435	−2.627	−2.041

lengths and angles are summarized in Tables VI and VII, respectively.

In the case of extreme Jahn-Teller distortion, the spin dimer analysis suggests that the J_4 interaction (along the 101 direction) is the largest interaction for both compounds and J_1 and J_5 with 2 orders of magnitude lower relative strength are the interactions which mediate the strong J_4 interaction in a three-dimensional magnetic ordering. J_2 and J_3 are negligible for both systems.

The fact that J_4 is the strongest interaction suggests that the interactions become more significant if the orbitals that accommodate the unpaired electrons are coplanar (Fig. 7). This approach results in a rather low dimensional magnetic structure, where the relative magnitudes of exchange interactions, $J_4 \gg J_1$ and J_5, for both compounds do not support geometrical magnetic frustration. This is in agreement with the experimental magnetic data for the Li_5OsO_6, but not with those of Li_4ReMgO_6 (Table VIII).

From the alternative approach, when the contributions of d_{xy}, d_{xz}, and d_{yz} to the exchange interactions are equally probable and the influence of the tetragonal compression is minimized, a very different result is found. In fact J_2, J_3, and J_4 which form triangles in the *ac* plane are the three dominant interactions now. In such cases, geometrical magnetic frustration is expected (Table IX).

The energy levels of the 6*d* orbitals obtained from the extended Hückel molecular orbital calculations for $[OsO_6]^{5-}$ and $[ReO_6]^{6-}$ are shown in Table X.

It is evident that the energy splitting between the lowest lying d_{xy} state to the next state for $[OsO_6]^{5-}$ is larger than that of $[ReO_6]^{-6}$, 0.189 eV compared to 0.081 eV. This indicates that the Os-based compound exhibits a stronger Jahn-Teller distortion and therefore is best described based on the first approach without magnetic frustration. On the other hand, Li_4MgReO_6 does not show a strong tendency toward tetragonal compression and results in more closely spaced energy states. Thus, the results of Table X are more relevant here, supporting the geometrical magnetic frustration and is in good accordance with the previously reported experimental investigations.[11]

The low temperature neutron diffraction data for Li_5OsO_6 did not show any extra peaks due to long-range magnetic ordering. This is disappointing but not unusual for such dilute systems (1 magnetic atom out of 12 atoms) with $S=\frac{1}{2}$. Therefore, it is impossible to propose a magnetic structure for Li_5OsO_6.

Note that the calculated transfer energies, $\langle \Delta e^2 \rangle$, are significantly larger for all J's for Li_4MgReO_6 relative to Li_5OsO_6. In addition, the size of Os^{7+} is smaller than that of Re^{6+}, which results in larger Hubbard U for Os^{7+}. Accordingly, the spin exchange interactions for Li_4MgReO_6 are expected to be larger than those of Li_5OsO_6. This observation is semiquantitatively consistent with the much larger, negative θ value for the Re-based system.

IV. SUMMARY AND CONCLUSIONS

The crystal structure of the ordered rocksalt type Li_5OsO_6 was reinvestigated, using room temperature powder neutron diffraction data. This compound crystallizes in the $C2/m$ space group with the lattice parameters $a=5.0472(1)$ Å, $b=8.7827(2)$ Å, $c=5.0079(1)$ Å, $\beta=109.777(2)°$. There is no mixing between Os^{7+} and Li^+ in the crystal structure. The material shows AFM long-range order below 40 K and a frustration index $f \sim 1$. Nonetheless, evidence for short-range, low dimensional, AFM correlations is found from both susceptibility and heat capacity data when entropy removal is taken into account. This behavior is different from that of the isoelectronic, isostructural compound, Li_4MgReO_6, which exhibits spin-glass behavior below 12 K and $f \sim 14$. Spin dimer analysis was performed to understand the origin of this remarkable contrast. The results were consistent with a frustrated triangular lattice model for the Re-based compound while a stronger tetragonal compression in Li_5OsO_6 encourages low dimensional magnetic correlations rather than geometrical magnetic frustration.

ACKNOWLEDGMENTS

We thank Paul Dube for his assistance in collecting magnetic susceptibility and heat capacity data. We appreciate fruitful discussions with Craig Bridges and Mario Bieringer. J.E.G. acknowledges the Natural Sciences and Engineering Research Council of Canada for the financial support of this work.

*Author to whom correspondence should be addressed.

[1] J. E. Greedan, J. Mater. Chem. **11**, 37 (2001).
[2] P. Fazekas and P. W. Anderson, Philos. Mag. **30**, 423 (1974).
[3] G. C. Mather, C. Dussarat, J. Etorneau, and A. R. West, J. Mater. Chem. **10**, 2219 (2000).
[4] K. Hirota, Y. Nakazawa, and M. Ishikawa, J. Phys.: Condens. Matter **3**, 4721 (1991).
[5] J. N. Ramires, J. R. Dahn, J. E. Greedan, C. V. Stager, G. Liu, I. Davidson, and U. VonSachen, J. Solid State Chem. **102**, 542 (1991).
[6] S. J. Clarke, A. J. Fowdes, A. Harrison, R. M. Ibberson, and M. J. Rossiensky, Chem. Mater. **10**, 372 (1998).
[7] L. Viciu, Q. Huang, E. Morosan, H. W. Zandbergen, N. I. Greenbaum, T. McQueen, and R. J. Cava, J. Solid State Chem. **180**,

1060 (2007).
[8] O. A. Smirnova, J. Solid State Chem. **178**, 1165 (2005).
[9] S. Derakhshan, H. L. Cuthbert, J. E. Greedan, B. Rahaman, and T. Saha-Dasgupta, Phys. Rev. B **76**, 104403 (2007).
[10] K. A. Regan, Q. Huang, and R. J. Cava, J. Solid State Chem. **178**, 2104 (2005).
[11] M. Bieringer, J. E. Greedan, and G. M. Luke, Phys. Rev. B **62**, 6521 (2000).
[12] K. E. Stizer, M. D. Smith, and H.-C. zur Loye, Solid State Sci. **4**, 311 (2002).
[13] A. S. Erickson, S. Misra, G. J. Miller, R. R. Gupta, Z. Schlesinger, W. A. Harrison, J. M. Kim, and I. R. Fisher, Phys. Rev. Lett. **99**, 016404 (2007).
[14] T. Betz and R. Hoppe, ZAAC **524**, 17 (1985).
[15] T. Betz and R. Hoppe, ZAAC **512**, 19 (1984).
[16] M. H. Whangbo, H. J. Koo, and D. J. Dai, J. Solid State Chem. **176**, 417 (2003).
[17] J. Ren, W. Liang, and M. H. Whangbo, Crystal and Electronic Structure Analysis Using CAESAR, http://www.primeC.com, 2005.
[18] H.-J. Koo, K.-S. Lee, and M.-H. Whangbo, Inorg. Chem. **45**, 10743 (2006).
[19] A. C. Larson and R. B. Von Dreele, General Structure Analysis System (GSAS), Los Alamos National Laboratory Report No. LAUR 2000: 86-748.
[20] B. H. Toby, J. Appl. Crystallogr. **34**, 210 (2001).
[21] J. S. Smart, *Effective Field Theory of Magnetism*, W. B. Saunders, Philadelphia, (1966).
[22] P. Schiffer and A. P. Ramirez, Comments Condens. Matter Phys. **10**, 21 (1996).
[23] M. E. Fisher, Philos. Mag. **7**, 1731 (1962).